Desalination and Water Treatment
www.deswater.com
doi: 10.5004/dwt.2021.26713

213 (2021) 303–310
February

Structural study of the hydrotalcite-carbon composite and its use for the removal of aqueous sulfate

Edinson Castellar Arroyo[a], Cesar Solano Polo[b], Johana Rodríguez-Ruiz[c], Eduardo Espinosa-Fuentes[d,*], Edgardo Meza-Fuentes[e]

[a]*Universidad de Cartagena, Cartagena de Indias, Colombia, email: ecastellara@unicartagena.edu.co*
[b]*Instructor, Servicio Nacional de Aprendizaje-SENA, Universidad de Cartagena, Cartagena de Indias, Colombia, email: casp61@hotmail.com*
[c]*Instructor and Researcher, Servicio Nacional de Aprendizaje-SENA, Universidad de Cartagena, Cartagena de Indias, Colombia, email: ji.rodriguez@misena.edu.co*
[d]*Universidad de Puerto Rico, Puerto Rico, Universidad Libre, Barranquilla, Universidad de Cartagena, Cartagena de Indias, Colombia, email: eduardo.espinosa.fuentes@gmail.com*
[e]*Assistant Professor, Universidad de Cartagena, Cartagena de Indias, Colombia, email: emezaf@unicartagena.edu.co*

Received 8 October 2019; Accepted 14 October 2020

ABSTRACT

This investigation centers in the synthesis of solids with adsorptive properties of porous carbons and selective like hydrotalcites. Activated carbons are materials widely used for the removal of pollutants. The combination with materials like hydrotalcites, increases its capacity to adsorb contaminants anionic of aqueous solutions. In this work, hydrotalcites supported on activated carbon were synthesized. The compounds were prepared at 5.0%, 7.5%, and 10.0% of MgO-Al_2O_3; on activated carbon. The solids were evaluation in the adsorption of sulfate anions in an aqueous solution, it shows a greater capacity of adsorption than the activated carbons without support, specifically more than 90%. This result is very relevant for the water filter industry, due that at low concentrations, usually ordinary materials do not adsorb with facility the sulfate. The removal of the sulfate anions was facilitated by the synthesis of hydrotalcite supported on activated carbon. The synthesized solids were characterized by X-ray diffraction, Fourier transform infrared, thermogravimetric analysis with differential scanning calorimetry, specific surface area measures by the Brunauer–Emmett–Teller method and pore size by the Barrett–Joyner–Halenda method. This confirms the presence of hydrotalcites supported on activated carbon. In all solids were presented mesoporous in the form of slits, others presented micropores like the solid CA-5.0D. These characteristics convert to this material in an adsorbent potential of sulfate anions in aqueous solutions.

Keywords: hydrotalcite, sulfate removal, activated carbon, adsorption, pollutants

* Corresponding author.

1. Introduction

The contamination of water sources has been one of the most important environmental problems that have affected our planet, therefore, it is an inevitable issue of discussion. This contamination is mainly caused by organic and inorganic ions, which are the product of industrial residues, domestic wastewater, and septic systems, among others [1]. One of the most common inorganic contaminants is sulfate ion, which is naturally encountered in almost all bodies of water used for humans for their consumption. Normally, the sulfate ion is introduced to groundwater bodies by entrainment and dissolution of the water that is absorbed by rocks and materials like sulfates or gypsum [2,3]. Normal sulfate levels in water can increase due to contamination from mines, windmills, landfills, sewers, and other artificial sources. The sulfate in concentrations superior to 300 mg L^{-1} can cause gastrointestinal problems in humans; therefore, an excess of sulfate in water destined for human consumption is not recommended [4,5]. Another problem associated with this ion is that in an aquatic medium it is reduced by some bacteria to hydrogen sulfide, which is highly toxic to very high concentrations. It is also attributed that it can contribute to the process of eutrophication, consuming the oxygen in the water and thus causing the death of aquatics species. Therefore, sulfate ion concentrations in potable water should be limited to established standards, the World Health Organization states that the maximum concentration permitted for SO_4^{2-} ion is 250 mg L^{-1}. Several methods have been developed for sulfate-contaminated waters treatment, including chemical precipitation [6], crystallization [7], ion exchange [8,9], biological treatments [10], and reverse osmosis [11]. However, these methods present low yields and are highly expensive, for this reason, it is necessary to consider new alternatives that have higher yields at a very low cost. Adsorption is one of the techniques aligned with this concept; it is considered the most promising due to the simplicity and flexibility of design, easy operation, and profitability [12]. Among the most used adsorbents, we have porous solids such as aluminum and magnesium oxides, also silica gel, aluminosilicates, zeolites, ceramics, and activated carbons [13]. In the case of activated carbon, this material is considered one of the most versatile for the removal of various contaminants [14]. However, its use is limited in the case of anionic contaminants due to the number of active sites for anion retention, so the combination of activated carbon with other types of materials can increase the removal of specific anionic pollutants. One type of material interesting to increase the anion retention capacity of the activated carbon are the layered double hydroxides (LDH), which are anionic clays that once calcined at low temperatures form mixtures of di-metallic oxides and tri-metallic oxides and in the presence of water and anions can be restructured in the initial phase of hydrotalcite type [15,16]. This phenomenon is known as the "structure memory effect", it occurs when LDH are calcined to remove most anions and interlaminar water molecules. Once the calcined material is in contact with a solution of water containing anions, the anions are reattached to the solid, which results in the reconstruction of the solid, producing LDH [17]. This work is centered on the removal of sulfate in an aqueous solution by means of derivatives of LDH supported in activated carbon, in addition, several parameters are optimized like the time of contact, the pH, the amount of adsorbent, the initial concentration of sulfate, and temperature.

2. Materials and methods

2.1. Preparation of adsorbent solids

Two solutions were used to synthesize LDH supported on commercial activated carbon; a solution *A* composed of the mixture magnesium nitrate hexahydrate [$Mg(NO_3)_2{\cdot}6H_2O$] and aluminum nitrate nonahydrate [$Al(NO_3)_3{\cdot}9H_2O$] and another solution *B* composed of potassium hydroxide (KOH) and potassium carbonate (K_2CO_3). Bearing in mind that in the end the concentrations of 5.0% (CA-5.0A), 7.5% (CA-7.5A), and 10.0% (CA-10.0A) of magnesium oxide + aluminum oxide ($MgO\text{-}Al_2O_3$) would be obtained on the surface of the activated carbon after the calcination process. For preparing the solid CA-5.0A, initially 24.7 g of activated carbon were impregnated with 7 mL of solution *A* so that the solution nitrates were located in the activated carbon pores, this mixture was carried to a rotary evaporator (Heidbad model Heizbad Hei-VAP) with a constant agitation at 80 rpm for 24 h. After this, it was dried at 373 K for a period of 8 h. Subsequently, 5 mL of solution *B* was added, and was carried to constant agitation in the rotary evaporator at 80 rpm for 24 h, after which it was dried for 8 h at 373 K. Posteriorly, the solids obtained were heated to a temperature of 573 K in the air atmosphere producing the collapse of the hydrotalcite-type structure followed by the formation of the oxides.

2.2. Characterization of solids

The synthesized solids were characterized using Fourier transform infrared spectroscopy (FTIR), X-ray diffraction (XDR), thermogravimetric analysis (TGA), differential scanning calorimetry (DSC), specific surface analysis (Brunauer–Emmett–Teller (BET) and Langmuir methods), and porosity analysis (Barrett–Joyner–Halenda (BJH) method). For the FTIR analyses, the samples were mixed in a proportion of 1% in weight with potassium bromide to obtain a tablet that was later carried to the Shimadzu equipment, IRAffinity model. The X-ray diffractogram was obtained in a Shimadzu equipment, model XDR-600, in a range of 10°–80° 2θ degrees, using the Cu Kα radiation, generated at 40 KV and 30 Ma. TGA/DSC analyses were carried out in a TA instrument, model SDT Q600. For TGA/DSC analyses, the samples were subjected to a heating speed of 10°C min^{-1}, at 303 K at the temperature at which the mass was kept constant. The measure of the surface area specific and the porosimetry by nitrogen adsorption at 77 K in a Micrometrics equipment, model ASAP 2020. Adsorption–desorption isotherms were obtained with different volumes of liquid nitrogen $p/p°$, before proceeding with the analysis, the solids were calcined at 423 K, in order to eliminate water and volatile material present in the solids.

2.3. Adsorption experiments

The adsorption experiments were carried out by adding 200 mg of each synthesized solid (CA-5.0D, CA-7.5D,

CA-10.0D) in 100 mL of sulfate solution at concentrations of 10, 20, 30, and 40 mg L^{-1}, the experiments were realized at a temperature of 298 K, pH 6, with a constant agitation at 500 rpm with a predetermined time intervals, in a magnetic stirrer model MS-H280-Pro, in which aliquots were obtained at different times. The sulfate concentration was determined by the turbidimetry technique using a nephelometer. The concentration was determined by taking samples every five minutes until a constant result was obtained.

3. Results and discussion

3.1. Characterization of solids

Fig. 1 shows the FTIR spectra of the uncalcined solids (CA-5.0A, CA-7.5A, and CA-10.0A), in all the solids is observed a wide band centered around 3,440 cm^{-1}, which is attributed to the stretching vibration of the hydroxyl group in the water molecules adsorbed on the surface of the materials [18]. The band observed at 1,640 cm^{-1} corresponds to the angular deformation of δ-HOH and is due to the water molecules present in the interlaminar layer of the synthesized solids. In addition, a peak associated with the antisymmetric stretching of the CO_3^{2-} ion appears in the central region of the spectrum around 1,383 cm^{-1}.

Fig. 2 shows the FTIR spectra of the calcined solids (CA-5.0D, CA-7.5D, and CA-10.0D) and activated carbon (CA). In the CA spectrum, a band between 3,300 and 3,500 cm^{-1} is observed, which is attributed to the stretching of the H···O···H bonds of the physisorbed water molecules on the surface, in relation to the calcined solids, a band appears at 1,510 cm^{-1} characteristic of the octahedron that forms the sheet for the Al–OH bond and at 470 cm^{-1} for the Mg–OH bond, which shows the formation of oxides in the activated carbon [19,20]. In all materials, a high band was observed around 1,440 cm^{-1}, which can be due to the presence of magnesium or aluminum carbonate on the internal surface of the materials.

The thermograms of the synthesized solids are presented in Fig. 3. In these, three steps of mass loss are observed: the first occurs below 373 K, and is shown a mass reduction of 14.60% for the CA-5.0A solid, 5.78% for the CA-7.5A solid, and 4.75% for the CA-10.0A solid, this mass loss is due to the release of physisorbed water on the surface and in the pores of the material; and in addition, this mass loss is associated with an endothermic peak between 353 and 373 K [21]. In the second interval, the mass reduction is associated with the collapse of the LDH structure within the activated carbon, this is caused by the exit of the interlaminar water and the beginning of dehydroxylation of the sheets and decarbonation of the interlaminar space, the exit of this product is obstructed, which causes carbon dioxide to reaction with the metal oxides present, forming transition carbonates that decompose at higher temperatures. In this second process, the formation of MgO begins, which has an energy requirement of around 22.46 J g^{-1} in the case of CA-5.0A; for CA-7.5A it required approximately 33.88 J g^{-1} and for CA-10.0A it required 37.85 J g^{-1}. The last mass loss is due to the combination of the carbonaceous material combustion process and the formation of magnesium and aluminum oxides.

Fig. 4 shows the adsorption–desorption isotherms of N_2 at 77 K of the different synthesized solids and the activated carbon used as support. The values of the textural parameters obtained by N_2 adsorption by BET and *t*-plot methods are shown in Table 1. The shape of the isotherms for all solids was type IV (IUPAC), with a significant nitrogen uptake at low relative pressure, indicating that the solids are microporous, however, a hysteresis cycle was presented in all graphs. The hysteresis cycles are of the H_4 type, which is associated with capillary condensation that occurs in the mesopores present in the materials [22]. Table 1 shows that CA solid, used as a support, has

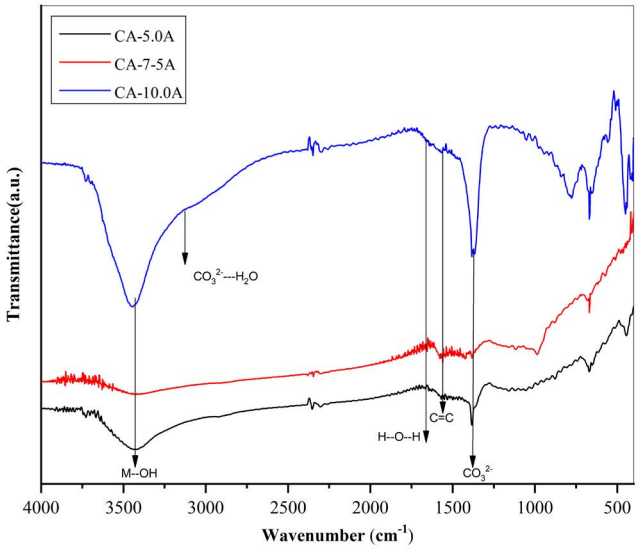

Fig. 1. FTIR spectra of the activated carbon and uncalcined composites materials at different percentage of hydrotalcite.

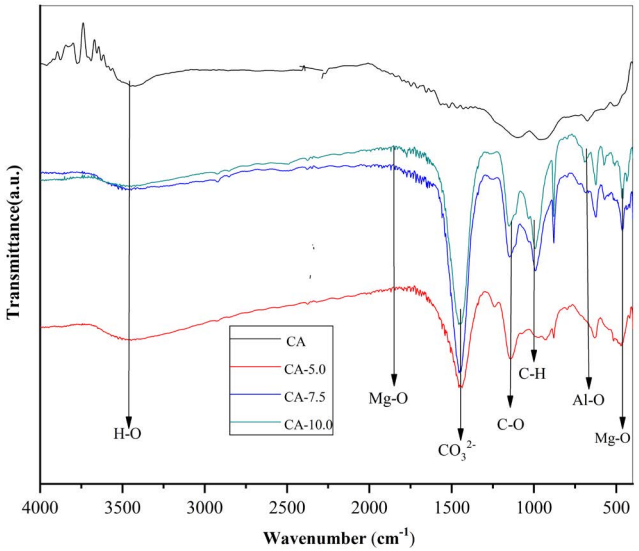

Fig. 2. FTIR spectra of the activated carbon and calcined composites materials at different percentage of hydrotalcite. Temperature of calcination was 423 K.

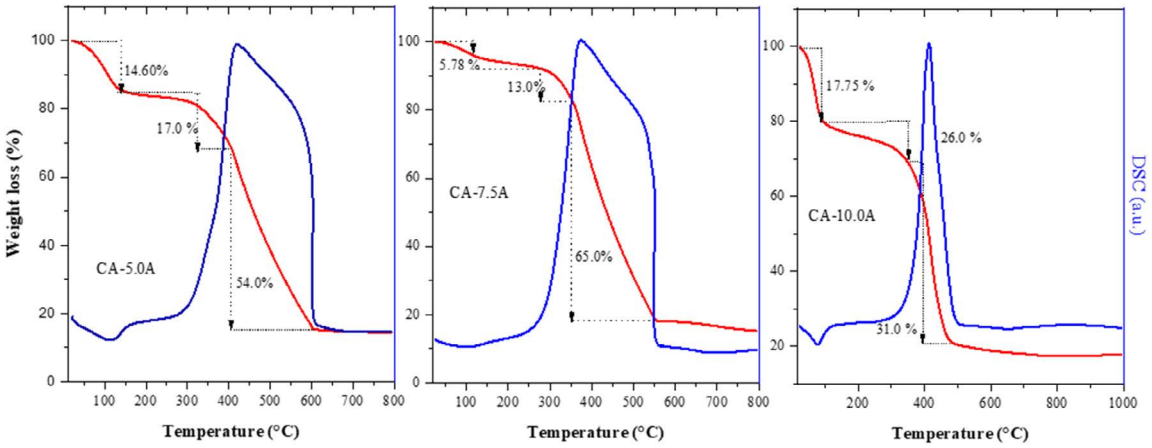

Fig. 3. TGA-DSC curves of the composite materials.

Table 1
Textural parameter obtained by the adsorption of N_2 a 77 K, using BET, and *t*-plot methods

Solid	Sg (m^2 g^{-1})	Micropore area (*t*-plot) m^2 g^{-1}	Pore volume (cm^3 g^{-1})	Pore diameter (Å)
CA	708	457	0.24	18.5
CA-5.0D	463	336	0.20	15.7
CA-7.5D	200	151	0.11	21.1
CA-10.0D	550	260	0.12	13.4

the highest specific surface area, which decreases in the synthesized solids due to the formation of LDH particles within the CA pores. The values of this parameter in the synthesized solids show notable differences among each other, a similar case occurs with the micropore area where it is observed that there are marked differences in all the solids, being the CA-5.0D material the least affected.

The solids CA-5.0D and CA-7.5D, showed the specific surface areas with the lowest values (463 and 200 m^2 g^{-1}) and with microporous volumes of (0.20 and 0.11 cm^3 g^{-1}), which means that the incorporation of LDH occurs preferably in pores of major dimension, which is reflected in a decrease of the external surface compared to the CA solid. In the case of the solid CA-10.0D a micropore surface of 260 m^2 g^{-1} and a micropore volume of 0.12 cm^3 g^{-1} are observed, these values permit us to guess that the incorporation of LDH occurs preferably in micropores of solids. The pore diameter values obtained by the BJH method for solids and the CA are shown in Table 1, and it can be observed that the CA-10.0D and CA-5.0D solids have the smallest pore diameter values, which is probably due to the content of LDH in its interior.

In general terms, it was observed that in the case of CA solid, 65% of that area is due to micropores, the rest is attributed to mesopores, which originate the hysteresis observed in the graph of adsorption–desorption of N_2. The specific surface area of the calcined materials changed with the incorporation of hydrotalcite. This parameter decreased in all cases, indicating that particles of hydrotalcite are incorporated in the pores. For example, in the solid CA-5.0D, its specific surface area decreased by approximately 35% with respect to the calcined carbon without the presence of hydrotalcite, and this can be attributed to the presence of particles associated with the decomposition of the hydrotalcite in the micropores and mesopores. This reduces the possibility of entry of N_2 during the adsorption process and, thereby, affecting the specific surface area.

In addition, the area attributed to micropores is 73% of the total area, and compared with solid CA, indicated that the location of particles of hydrotalcite was major in the mesopores. This was confirmed by the decrease in the diameter of the pores reported in the solid CA-5.0D. In the case of CA-7.5D, the presence of particles of hydrotalcite caused the obstruction of the majority of the pores of the carbon, which represented a decrease of 72% of the total surface area. In this case, particles of hydrotalcite were distributed in all types of the pores of carbon, exhibiting pores with major diameters than the other materials. The CA-10D registered a lower loss of specific surface area with respect to the CA. The results indicate that the loss of surface area is principally caused by a decrease in the surface area exposed by the micropores, in which particles of hydrotalcite probably were located. In addition, a small increase in the surface area of the mesopores is observed, which can be attributed to the formation of new pores due to the rapid liberation of water and carbon dioxide caused by the thermal decomposition of hydrotalcite.

The X-ray diffractogram showed peaks associated with the hydrotalcite-type phase and the graphite phase, which is characteristic of the activated carbon. Also, it

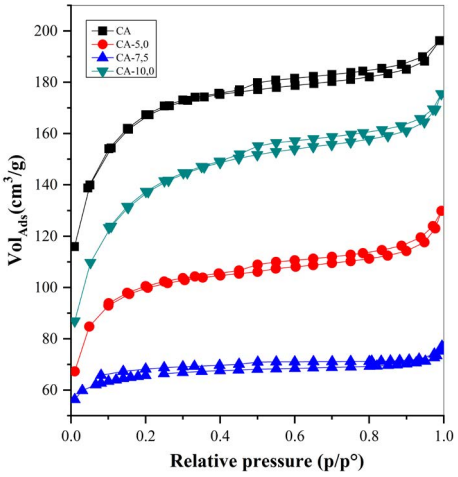

Fig. 4. Adsorption–desorption isotherm of the activated carbon and the calcined composite materials.

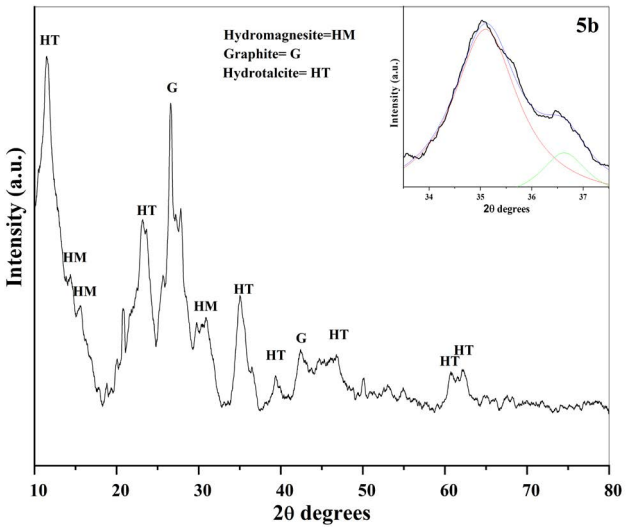

Fig. 5. (a) X ray-diffractogram of CA-5 solid, before calcining and (b) deconvolution of the peak corresponding to the plane (0 1 2) and statistical values associated with the peak separation process using a Lorentz-type regression.

was observed peaks of lower intensity associated with the hydromagnesite material, which indicates the formation of this compound during the preparation of the solids. The peaks of the hydrotalcite phase were intense and sharp, indicating the formation of particles of high crystallinity, confirming the effectiveness and the veracity of the method used (Fig. 5a). HDLs are lamellar solid, therefore many investigators consider that it is not applicable, because HDLs do not form spherical particles, so it is not possible to determine the distribution of its particles [23]. However, Scherrer's equation [24], is used for calculating the size of particles the solid CA-5.0A, considering the peak registered in 35.0 of the XRD spectrum, which corresponds to the plane (0 1 2). Previously to this calculation, it was carried out the deconvolution of the graph in the range of 33.5–37.5 to separate the peak corresponding to this plane of the interferences (Fig. 5b). The particle size was about 10.8 nm, which indicates that the hydrotalcite of this material is produced at the nanoparticle level.

3.2. Adsorption experiments

Adsorption experiments were carried out to determine the optimal conditions for the removal of sulfate in an aqueous solution with the different solids (CA, CA-5.0D, CA-7.5D, and CA-10.0D), and to determine the amount of sulfate removed by the adsorbents. Fig. 6, shows the percentages of sulfate removal in each of the solids synthesized and the activated carbon, in Fig. 6, it can be observed that all the solids adsorbed sulfate in different proportions. The percentage of removal in the equilibrium of the solids CA and CA-7.5D did not present great differences, which means that the presence of derivatives type hydrotalcite in a percentage of 7.5% on activated carbon does not contribute significantly to the adsorption of sulfate, by the contrary, it decreases the percentage of removal of the activated carbon because it decreases the specific surface of this material. The higher percentages of sulfate removal presented in the solids CA-5.0D and CA-10.0D, which implies that the adsorption is produced by the combination of the reconstruction of the structure type hydrotalcite and by a major time of the solution of sulfate with the inner walls of the activated carbon, which is favored by the minor diameter of the pores of the solids CA-5.0D and CA-10.0D, the solid CA-5.0D presents a mayor capacity of adsorption of sulfate at a concentration of 20 mg L^{-1}, which will be used as a point of reference for posterior studies.

With respect to the presence of other anions, sulfate can compete mainly with the anion CO_3^{2-}, since it is an anion that possesses a high charge in relation to its ionic radius, in addition the hydrotalcite are easily stabilized with the carbonate. With respect to anions of charge –1, do not expect much competition due to that the sulfate, which similar to the carbonate in its charge also stabilizes the structure formed. The results show that more than 90% of the sulfate can be removed using solutions of 20 mg L^{-1}, which indicates that the carbonate anion formed by the dissolution of CO_2 in water does not interfere significantly with the adsorption of the sulfate anion.

Finally, pure hydrotalcite is expected to adsorb more sulfate than the hydrotalcite supported in the activated carbon, but it results that the carbon reduces the impact that other contaminants can cause on the pure hydrotalcite, thus improving the adsorption process. In addition, the commercial cost of pure hydrotalcite is much higher than that of the solid proposed in this paper.

3.3. Effect of contact time

Fig. 7 shows the percentages of removal of sulfate in the function of the contact time at an initial concentration of 20 mg L^{-1}, at room temperature (298 ± 2 K), pH 6, and an amount of adsorbent of 200 mg CA-5.0D. It can be observed that sulfate adsorption is a fast process in the first 15 min, which means that adsorption is, kinetically, a very

fast process, while the adsorption equilibrium is obtained approximately in 40 min and the optimum contact time is 100 min. Sulfate removal is higher at the beginning of the graph due to the greater number of sites available for adsorption in the synthesized solid.

3.4. Effect of initial concentration

Fig. 7b shows the effect of the initial concentration of sulfate in the adsorption on the solid CA-5.0D. The experiments were carried out at room temperature (298 ± 2 K), pH 6, initial concentrations of 10–40 mg L^{-1}, with an amount of adsorbent of 200 mg, and contact time of 100 min. The results showed that the percentage of removal of sulfate decreased from 90% to 70%, this reduction in the capacity of adsorption is attributed to the lack of sites active required for the adsorption of sulfate at high concentrations. The higher sulfate adsorption capacity occurred at low concentrations and this is probably due to higher availability of active sites for a lower number of adsorbates [25].

3.5. Effect of adsorbent mass

Fig. 7c shows the effect of the amount of adsorbent CA-5.0D on the adsorption of sulfate in an aqueous solution. The amount of the adsorbent was varied between 50 and 200 mg, at temperature (298 ± 2 K), pH 6, with an initial concentration of sulfate of 20 mg L^{-1}. The result shows that the percentage of sulfate removal in the solid CA-5.0D increased rapidly with the increase in the mass of the adsorbent. This result is expected due to the increase in the amount of adsorbent conducive to higher availability of active sites. When the amount of adsorbent is increased from 50 to 200 mg, the percentage of adsorption of sulfate increased from 65% to 90% [26].

3.6. Effect of pH

The pH of the solution is a significant parameter that controls the surface properties of the adsorbent, like the charges of the surface and the ionic species of the adsorbate in an aqueous solution. With this in mind, the

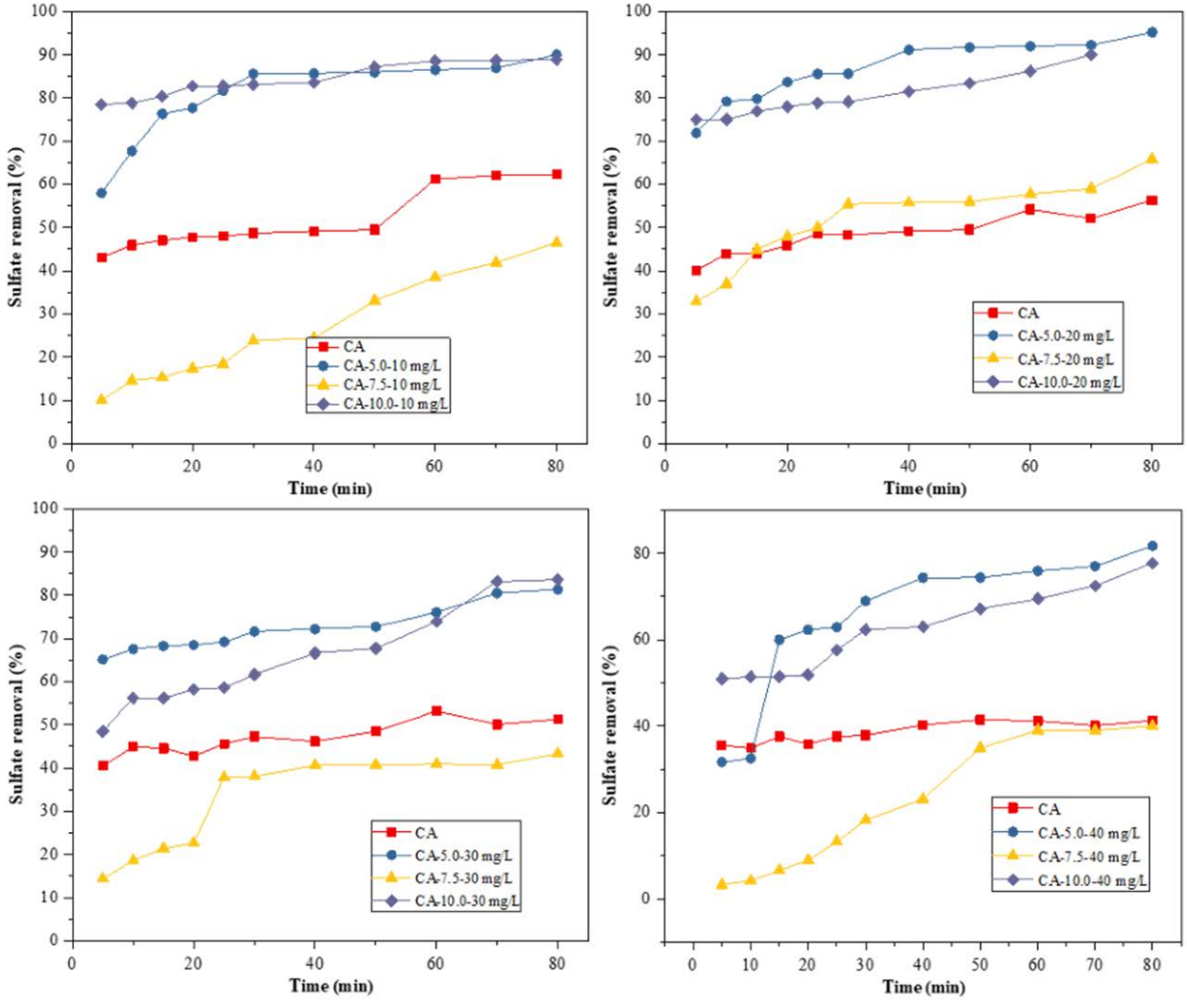

Fig. 6. Adsorption capacity of sulfate ions a function of time for each solid, from several starting concentration.

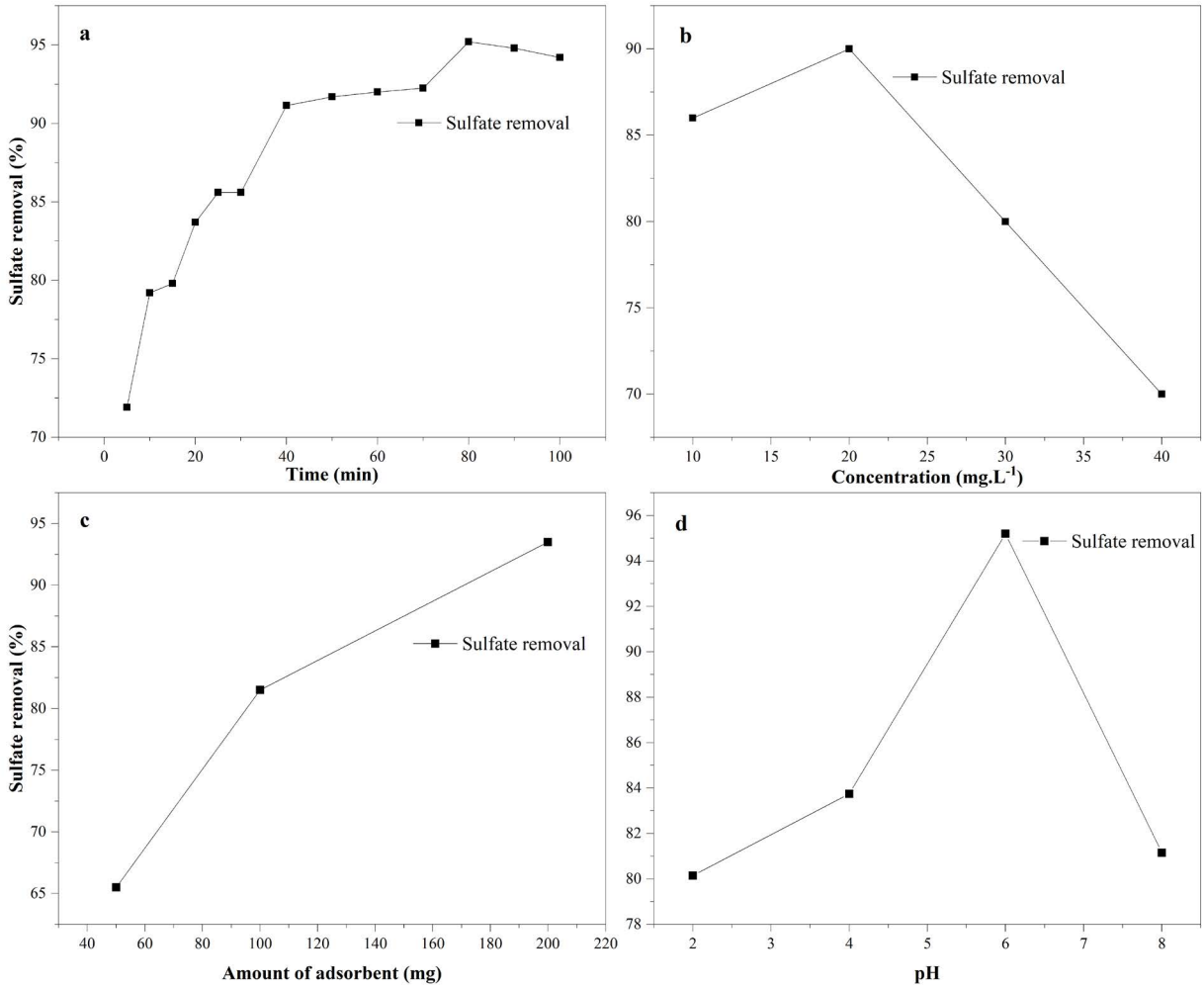

Fig. 7. Adsorption capacity of sulfate ions a function of: (a) contact time, (b) initial concentration on adsorption, (c) adsorbent mass on adsorption, and (d) pH.

adsorption capacity of the solid CA-5.0D was analyzed at different pH values varying from 2 to 8. Fig. 7d shows that the adsorption capacity increases with the increase of the pH and reaches a value maximum from 90% at pH 6, at lower pH values the capacity of adsorption decreases, probably at the dissolution of the HDL in an acid medium producing species Al^{3+} which interact strongly with the sulfate, which generates complexes soluble producing a decrease in the affinity of the sulfate with the adsorbent. At pH greater than 6 the capacity of adsorption decreases due to the competition of the groups OH^- for the sites active of the adsorbent [27].

3.7. Effect of temperature

The effect of temperature on adsorption experiments was studied at a range of temperatures from 298 to 323 K, pH 6, and amount of adsorbent (CA-5.0D) 200 mg in 100 mL of solution. The equilibrium contact time of adsorption was maintained at 100 min. The result is shown in Fig. 8, evidence that the percentage of adsorption decreases with the increase in the temperature from 90%

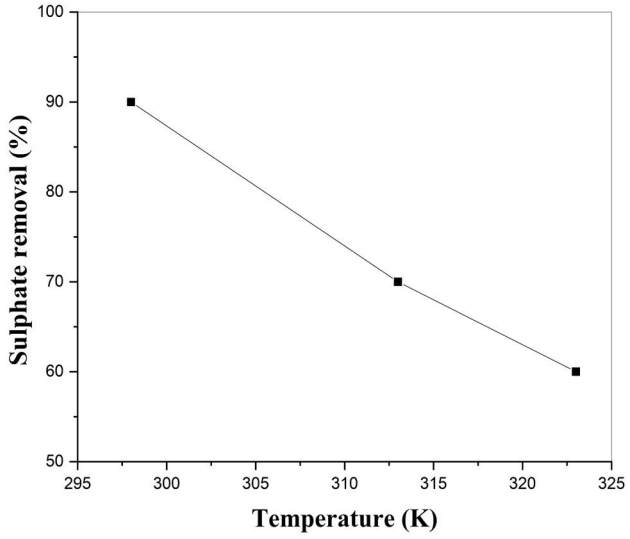

Fig. 8. Adsorption capacity of sulfate ions a function of temperature.

to 60%. This result revealed the exothermic nature of the adsorption processes [28].

4. Conclusion

The LDHs were synthesized with success in the pores of activated carbon, which was confirmed by the techniques of characterization FTIR, TGA/DSC, and XRD. The results of the experiments of adsorption permitted optimizing the parameters of adsorption of sulfate in aqueous solutions, that is, the contact time, pH, mass of the adsorbent, the amount of sulfate adsorbed, and temperature. Results showed that the greatest percentage of sulfate removal occurred at a concentration of 20 mg L^{-1} with the solid CA-5.0D obtaining a value from 90%, it was observed that the optimal amount of the adsorbent is 200 mg, at pH 6 and 100 min of contact time to reach the equilibrium. With these results, it can be concluded that the solid CA-5.0D is useful and very economic for the removal of the sulfate in an aqueous solution.

References

[1] J. Wang, J. He, H. Chen, Assessment of groundwater contamination risk using hazard quantification, a modified drastic model and groundwater value, Beijing Plain, China, Sci. Total Environ., 432 (2012) 216–226.

[2] H. Huan, B.T. Zhang, H. Kong, M. Li, W. Wang, B. Xi, G. Wang, Comprehensive assessment of groundwater pollution risk based on HVF model: a case study in Jilin City of northeast China, Sci. Total Environ., 628–629 (2018) 1518–1530.

[3] D. Wilson, A. Fernández, Y. Zayas, Development and validation of an anemometric titration method for the determination of the sulphate ion in natural and waste water samples, Rev. Cub. Qca., 19 (2007) 28–33.

[4] E. Nariyan, C. Wolkersdorfer, M. Sillanpá, Sulphate removal from acid mine water from the deepest active European mine by precipitation and various electrocoagulation configurations, J. Environ. Manage., 227 (2018) 162–171.

[5] F. Li, J. Zhu, X. Deng, Y. Zhao, S. Li, Assessment and uncertainty analysis of groundwater risk, Environ. Res., 160 (2018) 140–151.

[6] C.T. Benatti, C.R.G. Tavares, E. Lenzi, Sulphate removal from waste chemicals by precipitation, J. Environ. Manage., 90 (2009) 504–511.

[7] S. Tait, W.P. Clarkeb, J. Keller, D. Batstonea, Sulphate removal from wastewater by mixed oxide-LDH, J. Water Res., 43 (2009) 762–772.

[8] E. Nixdorf, Y. Sun, M. Lin, O. Kolditz, Development and application of a novel method for regional assessment of groundwater contamination risk in the Songhua River Basin, Sci. Total Environ., 605–606 (2017) 598–609.

[9] C.A. Basha, S.J. Selvi, E. Ramasamy, S. Chellammal, Removal of arsenic and sulphate from the copper smelting industrial effluent, Chem. Eng. J., 141 (2008) 89–98.

[10] J.P. Maree, H.A. Greben, M. Beer, Treatment of acid and sulphate-rich effluents in an integrated biological/chemical process, Water SA, 30 (2004) 183–189.

[11] J.H. Ahn, K.H. Choo, H.S. Park, Reverse osmosis membrane treatment of acidic etchant wastewater: effect of neutralization and polyelectrolyte coating on nitrate removal, J. Membr. Sci., 310 (2008) 296–302.

[12] V.K. Gupta, I. Ali, V.K. Saini, Adsorption studies on the removal of vertigo blue 49 and orange DNA 13 from aqueous solutions using carbon slurry developed from a waste material, J. Colloid Interface Sci., 315 (2007) 87–93.

[13] S. Montoya-Suarez, F. Colpas-Castillo, E. Meza-Fuentes, J. Rodríguez-Ruiz, R. Fernandez-Maestre, Activated carbons from waste of oil-palm kernel shells, sawdust and tannery leather scraps and application to chromium (VI), phenol, and methylene blue dye adsorption, Water Sci. Technol., 73 (2016) 21–27.

[14] O. Primera-Pedrozo, F. Colpas-Castillo, E. Meza-Fuentes, R. Fernández-Maestre, Activated carbons from sugar cane bagasse and corn husk for the adsorption of cadmium and lead, Rev. Acad. Colomb. Cienc. Exact. Fís. Nat., 35 (2011) 387–396.

[15] F. Cavani, F. Trifiro, A. Vaccari, Hydrotalcite-type anionic clays: preparation, properties and applications, Catal. Today, 11 (1991) 173–302.

[16] J. Rodríguez-Ruiz, S. Osorio-Herrera, E. Meza-Fuentes, Effect of zinc substitution by nickel on hydrotalcite-type solids, Matéria, 25 (2020) 1–10.

[17] E. Meza-Fuentes, J. Rodríguez-Ruiz, C. Solano-Polo, M. Rangel, A. Faro, Monitoring the structural and textural changes of Ni-Zn-Al hydrotalcites under heating, Thermochim. Acta, 687 (2020) 1–9, doi: 10.1016/j.tca.2020.178594.

[18] G.Z. Kyzas, K.A. Matis, Nanoadsorbents for pollutants removal: a review, J. Mol. Liq., 203 (2015) 159–168.

[19] J. Kloprogge, D. Wharton, L. Hickey, R. Frost, Infrared and Raman study of interlayer anions CO_3^{2-}, NO_3^-, SO_4^{2-} and ClO_4^- in Mg/Al-hydrotalcite, Am. Mineral., 87 (2002) 623–629.

[20] H. Schaper, J. Berg-Slot, W. Stork, Stabilized magnesia: a novel catalyst (support) material, Appl. Catal., 54 (1989) 79–90.

[21] X. Ruan, S. Huang, H. Chen, G. Qian, Sorptión of aqueous organic contaminants onto dodecyl sulphate intercalated magnesium iron layered double hydroxide, Appl. Clay Sci., 72 (2013) 96–103.

[22] K.S.W. Sing, D.H. Everett, R.A.W. Haul, L. Moscou, R.A. Pierotti, J. Rouquerol, T. Siemienewska, Reporting physisorption data for gas/solid systems, with special reference to the determination of surface area and porosity, Pure Appl. Chem., 57 (1985) 603–619.

[23] U. Costantino, V. Ambrogi, M. Nocchetti, L. Perioli, Hydrotalcite-like compounds: versatile layered hosts of molecular anions with biological activity, Microporous Mesoporous Mater., 107 (2008) 149–160.

[24] E. Meza-Fuentes, J. Rodriguez-Ruiz, M. Rangel, Characteristics of NiO present in solids obtained from hydrotalcites based on Ni/Al and Ni-Zn/Al, Rev. Fac. Nac. Minas. DYNA, 86 (2019) 58–65.

[25] A. Halajnia, S. Oustan, N. Najafi, A.R. Khataee, A. Lakzian, Adsorption–desorption characteristics of nitrate, phosphate and sulphate on Mg–Al layered double hydroxide, Appl. Clay Sci., 80 (2013) 305–312.

[26] W.L. Yan, R. Bai, Adsorption of lead and humic acid on chitosan hydrogel beads, Water Res., 39 (2005) 688–698.

[27] W. Zhou, B. Gao, Q. Yue, L. Liu, Y. Wang, Al-Ferron kinetics and quantitative calculation of Al(III) species in poly-aluminum chloride coagulants, Colloids Surf., A, 278 (2006) 235–240.

[28] E. Wibowo, M. Rokhmat, M. Abdullah, Reduction of seawater salinity by natural zeolite (Clinoptilolite): adsorption isotherms, thermodynamics and kinetics, Desalination, 409 (2017) 146–156.